# The data and the beautiful (and sometimes surprising) math used to describe complex systems

Marcos G. E. da Luz[§]

**V Escola de Verão de Física de Curitiba – 2024**
**Programa de Pós-Graduação em Física**
**Universidade Federal do Paraná - UFPR**
09/02/2024



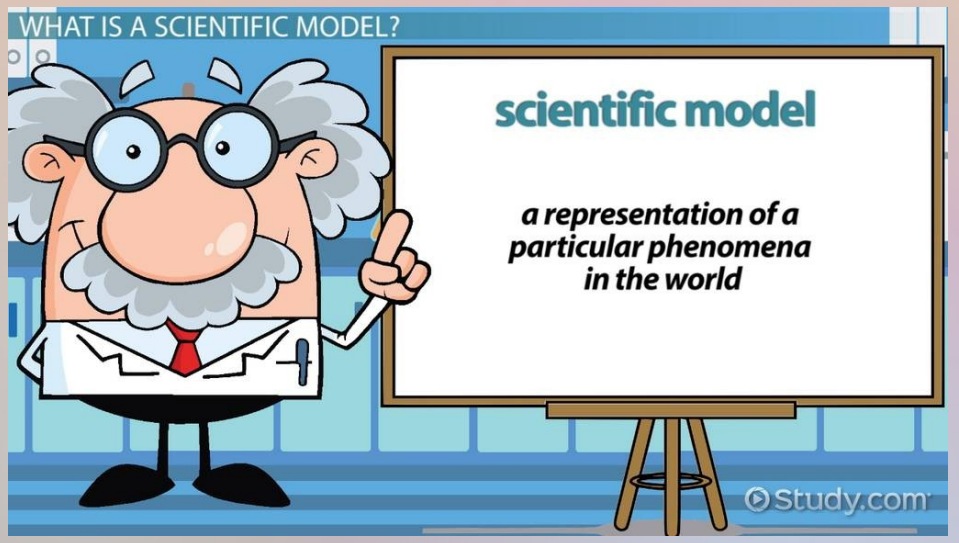


[§]Universidade Federal do Paraná-UFPR
Curitiba-PR, Brazil

# Group on complexity, disorder and non-linearity in classical and quantum systems

Somewhere in the Andes “altiplanes”, ~ 4.000 m above sea level




Physics Department
Universidade Federal do Paraná
Curitiba-PR, Brazil
luz@fisica.ufpr.br

Science is divided into big areas, but Nature is not! Thus, although physicist by training, our interest covers many different subjects, those in which complexity, non-linearity and disorder play fundamental roles. For that, mathematics is the right way to go. Not only because it is the proper language of science, but also because it is beautiful!!!! But never forgetting the real stuff, the lab!!!!

**Research interests**

1) Traditional physics: fundamental and mathematical aspects of quantum mechanics and statistical physics

2) The chemical-physical properties of organic macromolecules (like polymers), nano-structured and disordered materials and applications (e.g. in energy)

3) The relation between complexity and out-of-equilibrium processes in physics, ecology, chemistry, geology, etc. Examples:
- Dynamical and stochastic aspects of different phenomena
- Spatio-temporal pattern formation in biology
- Non-linear systems control

# Outline

- What type of science (based on physics) do you like to do?
- Three examples of data-oriented modeling
- When the mathematics you use is a bit different from that in your courses!

# Levels of Description of Nature (hierarchy and emergence)

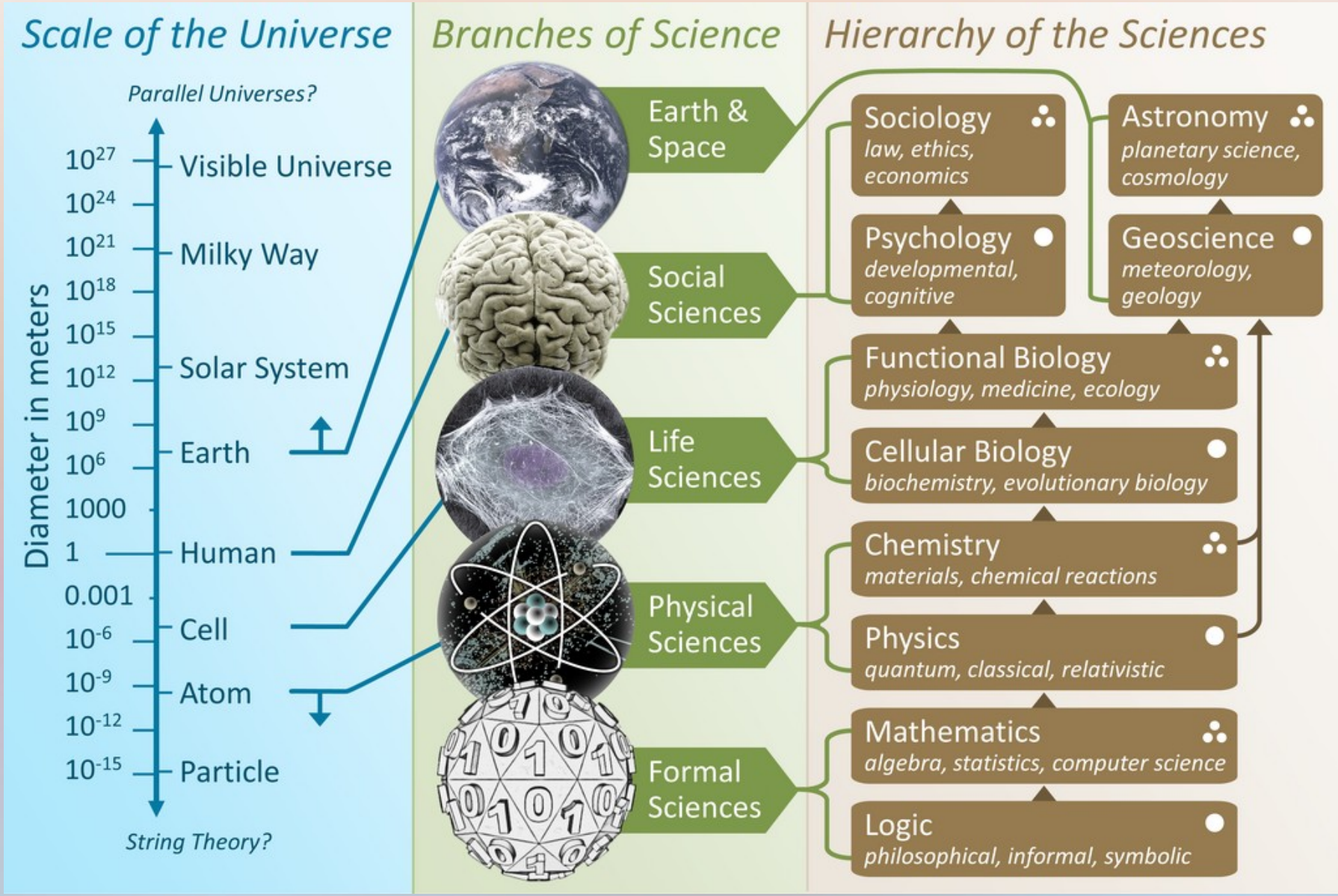

# Data!!!!!!!!!!!!!!!!!!!!!

1)  Jason and the Argonauts

2) Looking for the tube!



3) The Doors of Perception



“If the doors of perception were cleansed every thing would appear to man as it is, infinite”

William Blake

# Malaria in Numbers

https://www.cdc.gov/malaria/malaria_worldwide/impact.html

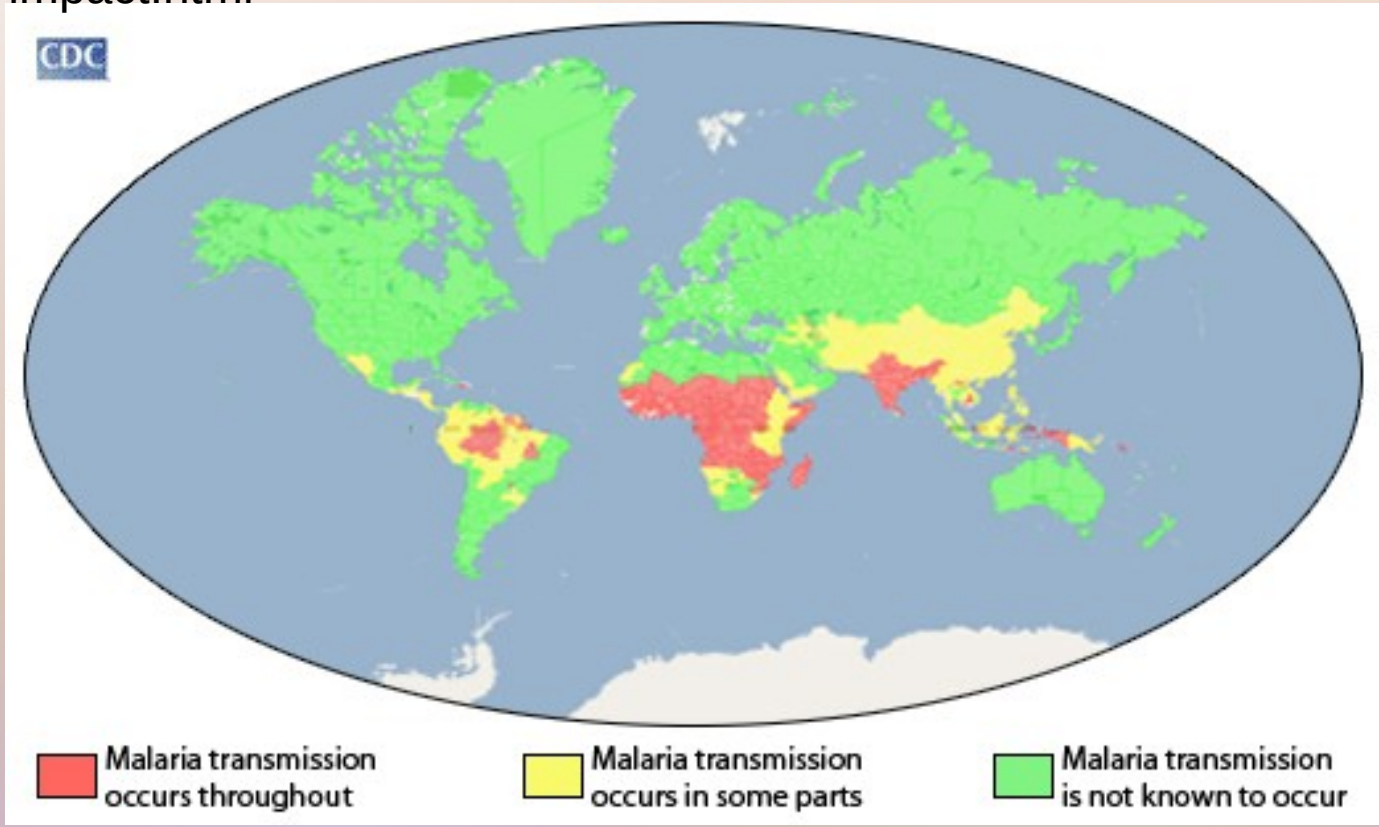


Malaria is one of the most severe public health problems worldwide. It is a leading cause of death and disease in many developing countries. Main victims: children and pregnant women.

**2021 Malaria Report**:

Nearly 1/2 the world's population lives in areas at risk of malaria: 87 countries and territories.

In 2020, it caused about 241 million clinical episodes, and 627,000 deaths.

Around 95% of deaths in 2020 were in Africa.

Costs (e.g., illness, treatment, premature death) are at least US $12 billion per year. The cost in lost economic growth is many times more than that.

Brazil (2021) 139.211

# Plasmodium sporozoite search strategy to locate hotspots of blood vessel invasion

P. Formaglio, M. E. Wosniack, R. M. Tromer, J. G. Polli, Y. B. Matos, H. Zhong, E. P. Raposo, M. G. E. da Luz, R. Amino
Nat. Commun. 14 (2023) 2965

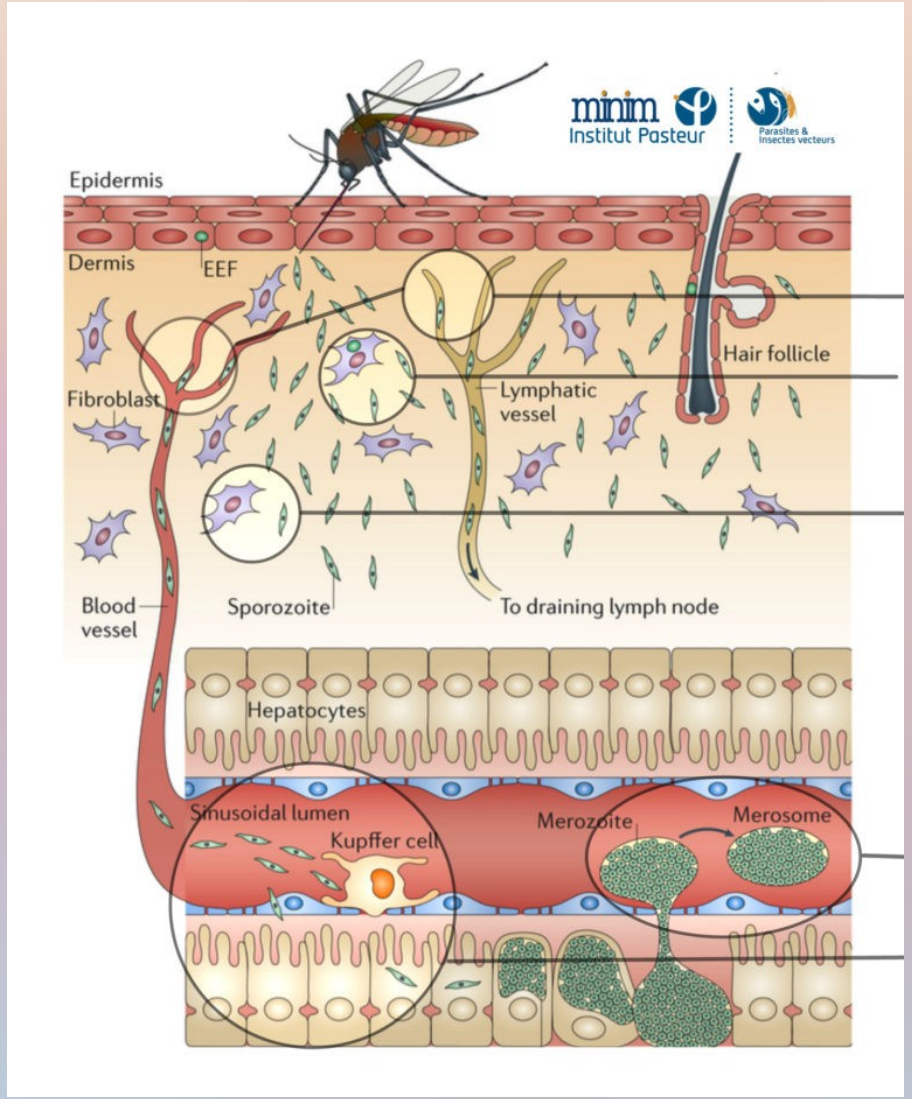

# Malaria Cycle

https://www.news-medical.net/life-sciences/The-Malaria-Parasite-Life-Cycle.aspx

https://mauziovarella.uol.com.br/doencas-e-sintomas/malaria/

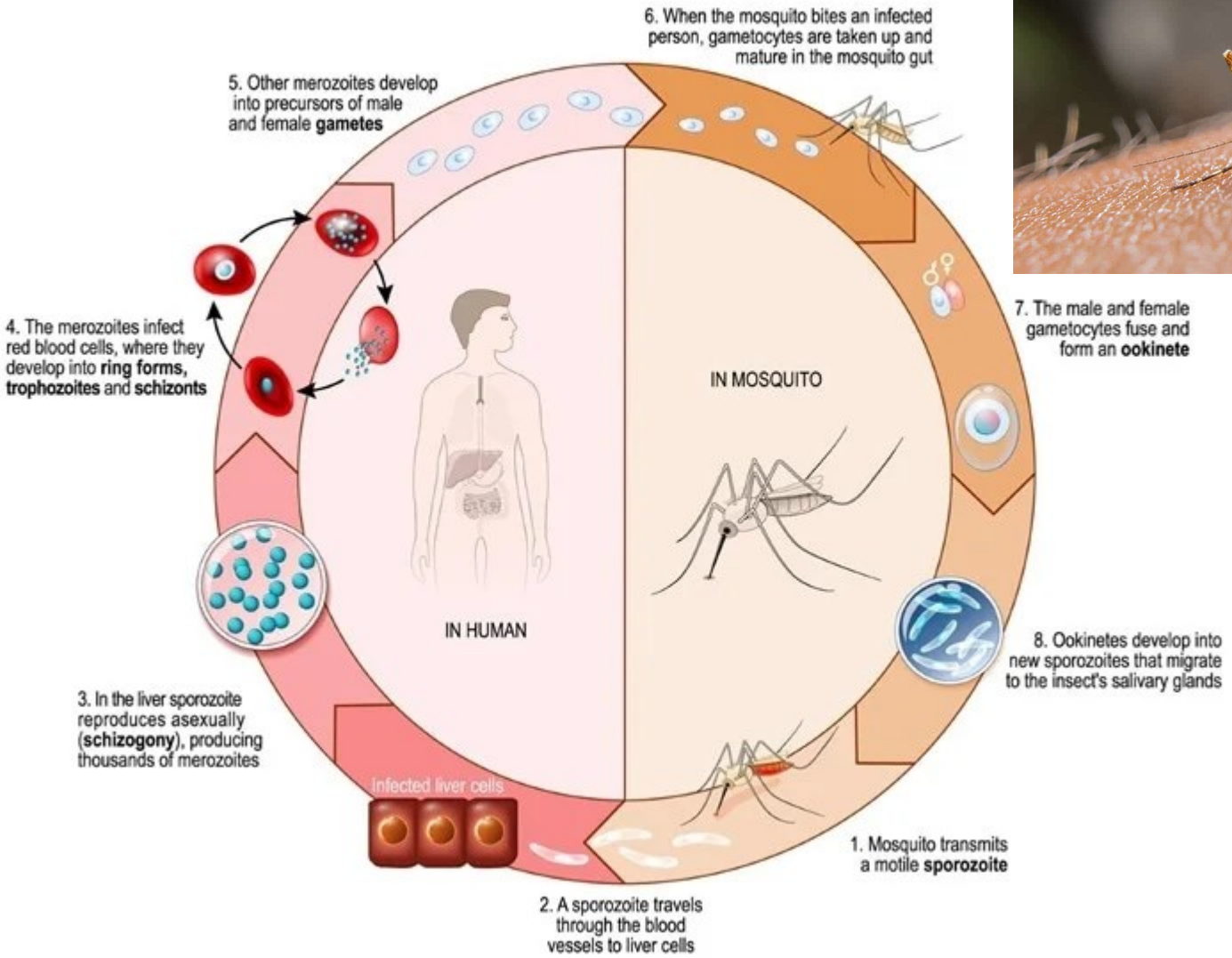




Anopheles



Plasmodium

# Analysis Methods

1) Tracked 400 (100+300) individuals, typically 40 minutes, two scales:
volume 320 x 320 x 30 $\mu m^3$ volume of 664 x 901 x 30 $\mu m^3$

2) Two-state Hidden Markov Model (HMM) to analyze the data. A HMM hypothesizes that the observable states of the system being modeled, which can be described by empirical measurements, evolve according to an underlying unobservable "hidden" stochastic process.

3) Hurst exponent H is a convenient measure of diffusiveness, where one has that the mean square displacement MSD (or $< x^2 >$) goes with

$$MSD \sim t^{2H}$$

Typically $H < 0.5$ (sub-), $H=0.5$ (normal), and $H > 0.5$ (super-) diffusion.

4) For the trajectories data analysis, frequently time windows of $\tau$ , from 4 seconds (equipment resolution) to 80 seconds, were used

# Analysis Methods (Cont.)

5) Truncated power-law distribution of the step length $\ell_{min} \leq \ell \leq L$:

$$P(\ell) \sim C / \ell^{\mu}$$

Decreasing $\mu$ within $1 < \mu < 3$ leads to an increasing degree of super-diffusiveness, as shown in the figure.

Observe the three limits, ballistic-like behavior, super-diffusive and normal diffusion as the exponent $\mu$ increases

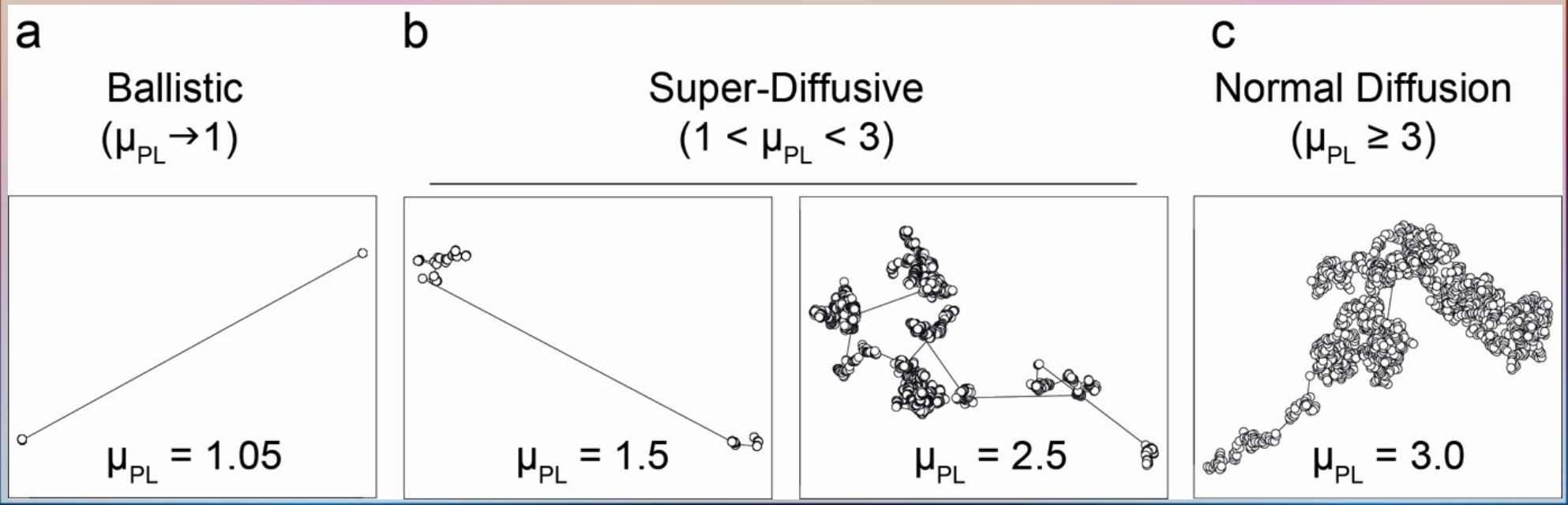

# Results

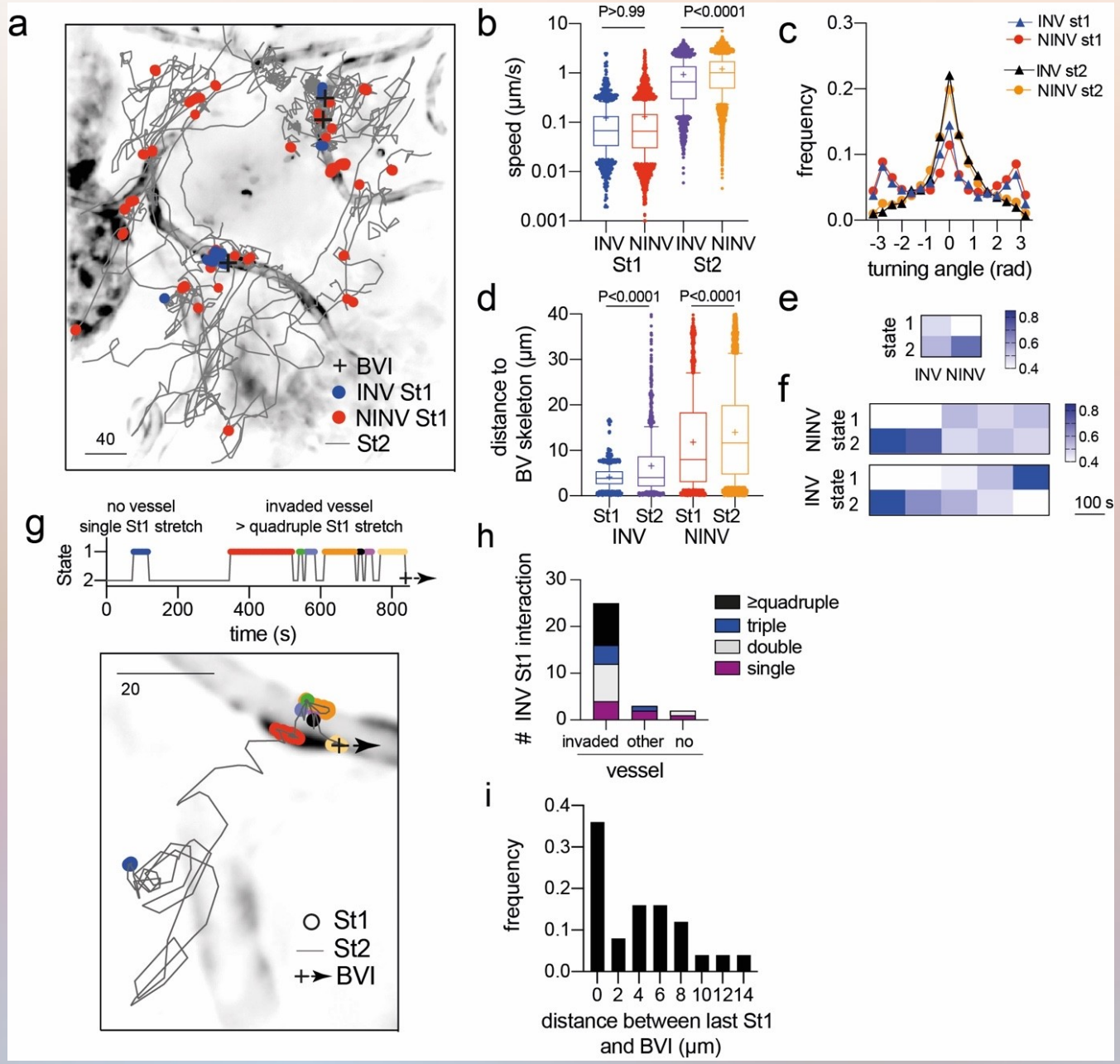


**Hidden Markov Model (HMM) analysis of sporozoite motility.** (a) Typical parasite tracks (scale: 40 µm) showing state 1 motility (St1, circles) of BV invaders (INV, blue) and non-invaders (NINV, red). (b) Sporozoite velocity. (c) Frequency of sporozoite turning angles. (d) Distance to the nearest BV according to HMM states. (e) INV/NINV HMM states distribution. (f) State frequencies over time. (g) Example of successive INV St1 interactions. (h) Number of INV displaying St1-stretches close (invaded vessel) or far (other vessel) from BVI. (i) Frequency distribution of distance between the last INV St1 and BVI..

# Results

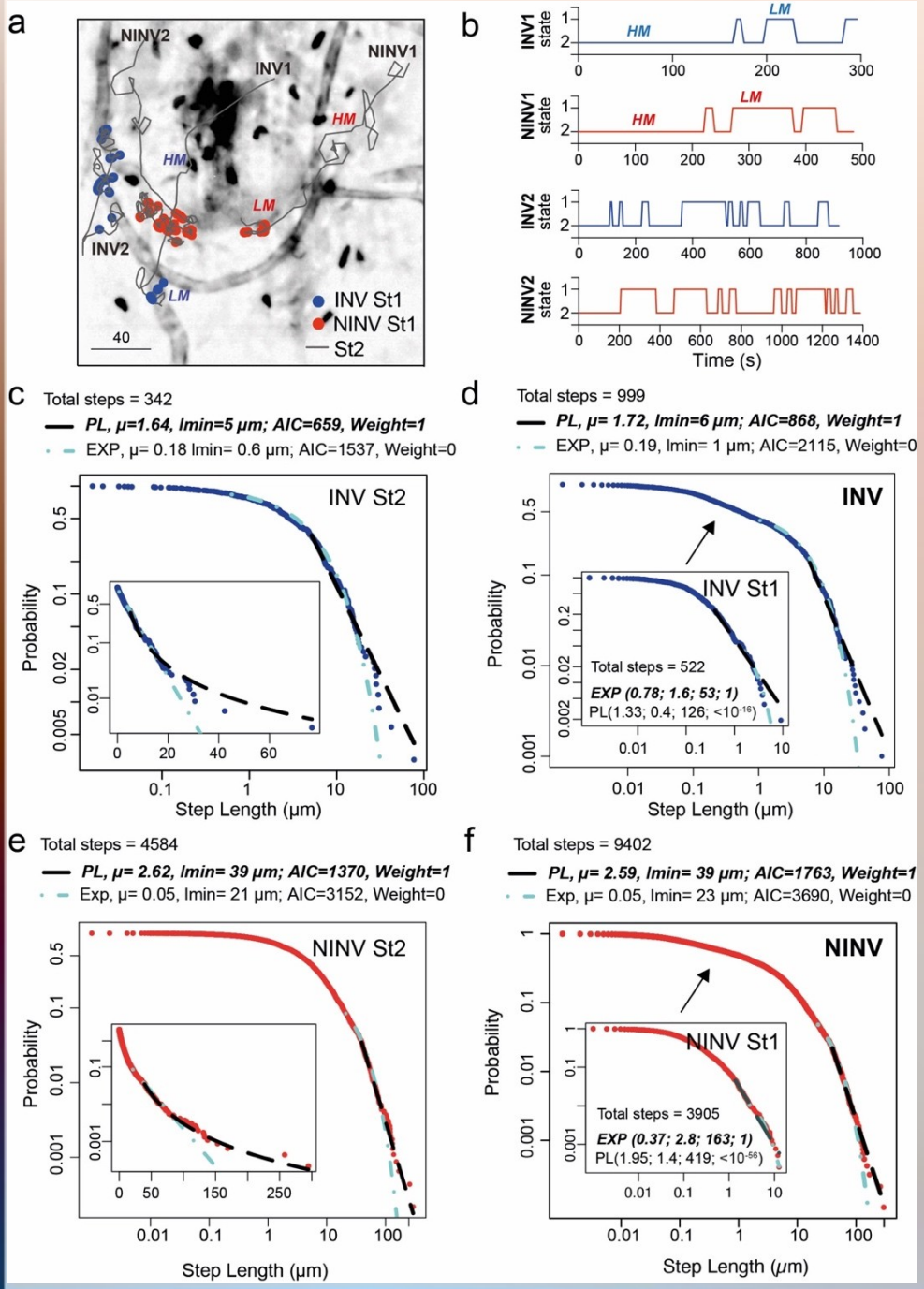


**High-motility mode and Lévy walk**. (a) Representative examples of INV (blue) and NINV (red) parasite tracks showing continuous segments of St2 high-motility (HM, lines) and St1 low-motility (LM, circles). Scale bar, 40 μm. (b) HM and LM state alternation over time for two INV and two NINV exemplary trajectories. (c-f) The best PL and EXP fits of, (c) INV parasites just in the St2 mode, (d) INV parasites combining the St1 and St2 modes (inset: only St1 mode is shown), (e) NINV parasites in the St2 mode (f), NINV parasites combining the St1 and St2 modes (inset: only St1 mode is shown). The insets in (c) and (e) display log-normal plots of the St2 mode, helping to highlight the long-tail distribution of the experimental data. Circles show empirical data, whereas dashed (black) and dotted-dashed (cyan) lines represent the best PL and EXP fits. The adjusted parameters μ and ℓmin as well as the total number of steps analyzed are indicated on each graph. Akaike Information Criterion (AIC) values and weight indicate the best fit highlighted using bold italic letters for each dataset. In the insets in (d) and (f), the numerical values correspond to (μ; ℓmin; AIC value, AIC weight).

# Results

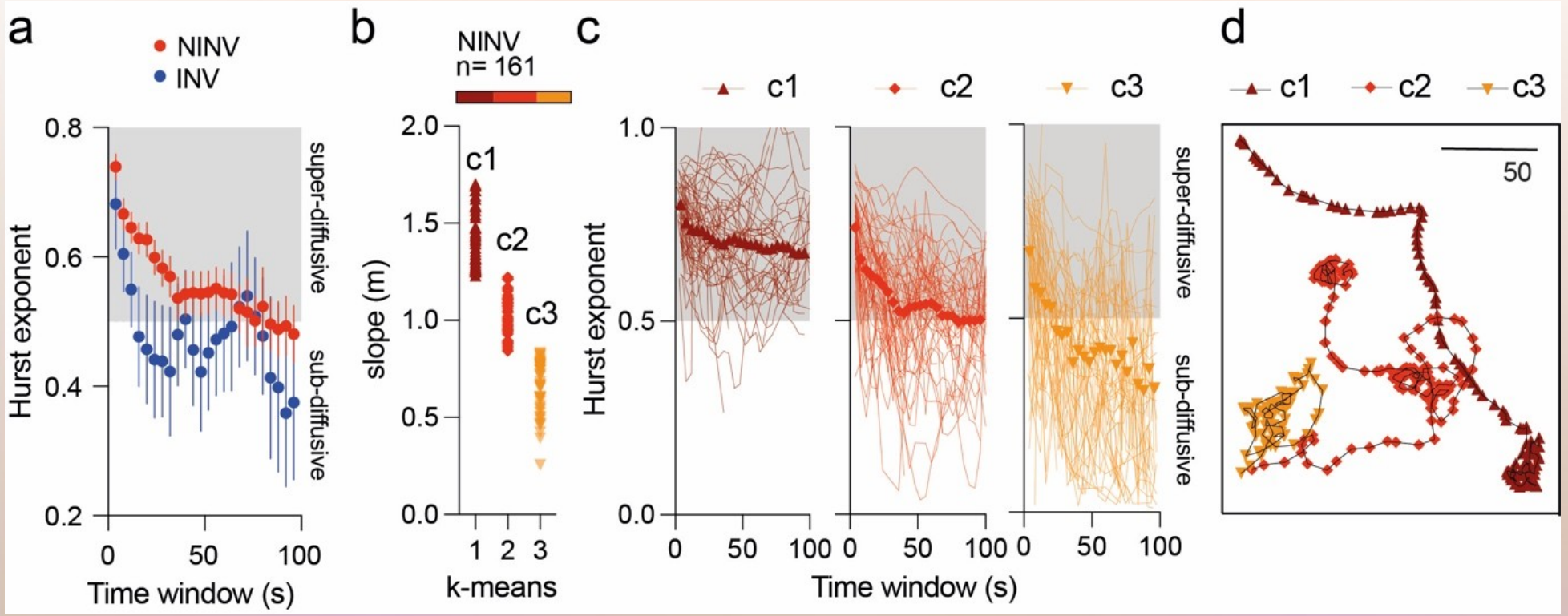


**Anomalous diffusive behavior of sporozoites.** (a) Hurst exponent of BV invaders (INV, blue circles) and non-invaders (NINV, red circles). Symbols: average of sporozoites from experiments. (b) k-means clustering of the slope (m) of MSD plotted in log-log scale against the analysis time window for the NINV population. Top graph represents the parasite percentage in each cluster. (c) Hurst exponent time series for sporozoites from clusters c1, c2 and c3. (d) Examples as shown in c. of a super-diffusive, forward moving parasite (c1), a sub-diffusive, meandering, circularly moving parasite (c3), and an intermediate behavior between the two previous phenotypes (c2).

# Results

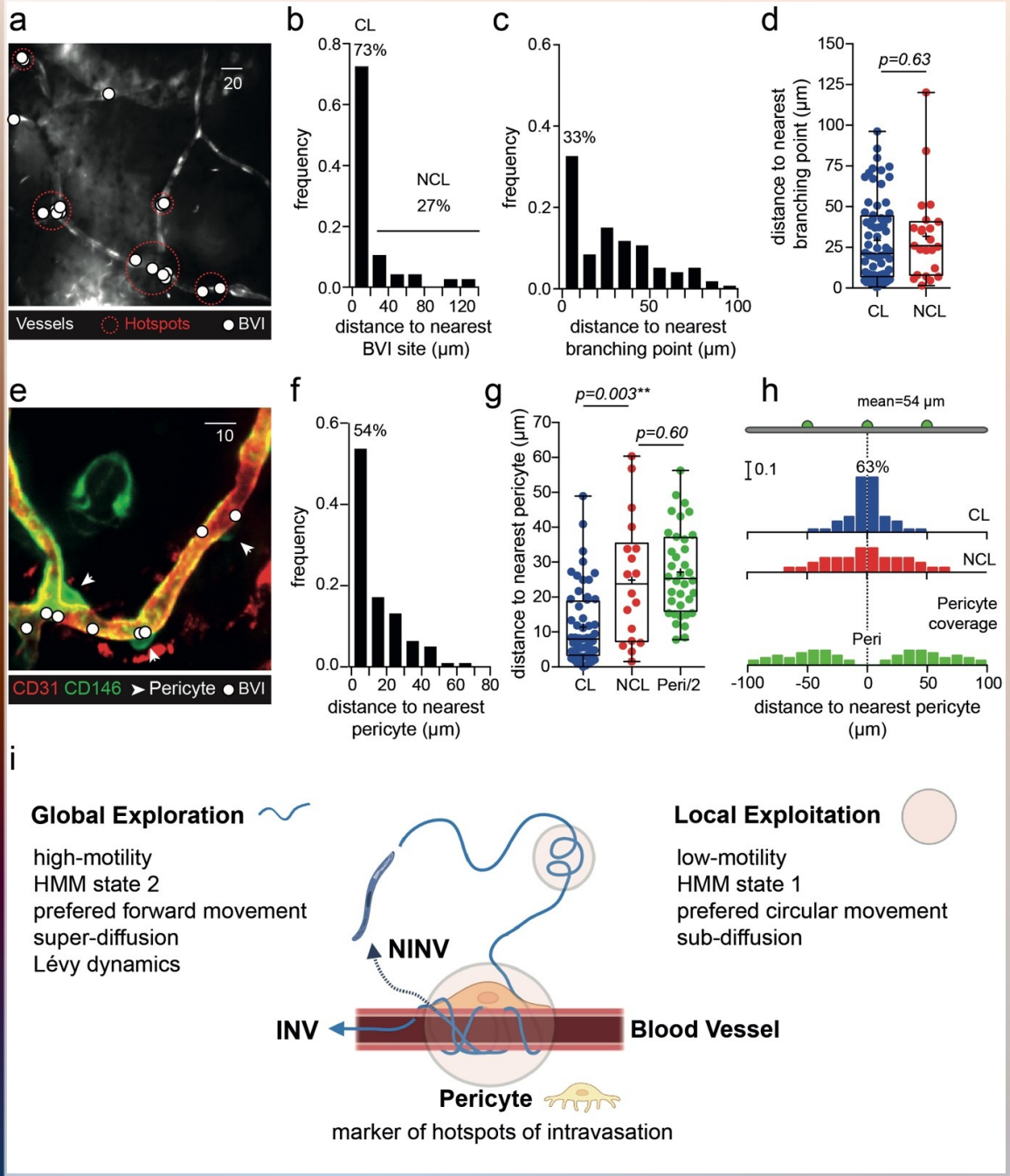


**Invasions at pericytes.** (a) Distribution of BVI (white). Bar 20 µm. (b) Distance between sites of BVI and their nearest neighbor. (c) Distance between sites of BVI and the nearest vascular branching points. (d) Distance between the sites of BVI and nearest branching points for CL and NCL invasions. (e) Distribution of $CD146^{+}$ (green) $CD31^{-}$ (red) pericytes (arrowheads) and clustered BVI (white). Bar 10 µm. (f) Diistances separating BVI from the nearest pericyte. (g) Distance between BVI and the nearest pericyte in CL (blue) and NCL (red). (h) BVI and pericyte distribution. (i) Search strategy.

# Summarizing: Global and local intermittent search strategy to find intravasation hotspots

The sporozoite BV search and invasion dynamics can be described as the following;

Once in the skin, sporozoites start moving in a superdiffusive, Lévy-like, high-motility mode. This behavior is consistent with a global exploratory search, seeking efficiently to encounter a BV.

Upon BV encounter, sporozoites switch to a subdiffusive low-motility mode with an important circular component. This change is compatible with local vessel exploitation, which allows for more careful scanning of a limited region of BV while probing for a permissive entry site in the microvasculature, associated with the presence of pericytes.

If, after some time, intravasation is not achieved, sporozoites tend to shift back to the superdiffusive mode, until finally invading a BV.

Why pericytes? It might directly or indirectly guide sporozoites to these hotspots of invasion or simply highlight weaker points for passage across the endothelial barrier.

# Summarizing: Global and local intermittent search strategy to find intravasation hotspots (cont.)

The plasmodium alternation between a global exploration and a local exploitation strategy is a pattern observed in many other biological search processes. For instance,  bumblebees use it to learn about proper foraging routes, optimizing energetic costs.

In fragmented landscapes, this alternation may also be a mandatory survival behavior for small predators, being themselves prey to other larger predators.

At a subcellular level, switching between 3D exploratory diffusion and 1D Brownian scanning exploitation, known as enhanced diffusion, can improve the efficiency of DNA binding proteins to find specific sequences in DNA strands.

Hence, sporozoites, grounded on the capacity to move forward and circularly, seem to have evolved a search strategy where they alternate between a global superdiffusive, Lévy-like high-motility mode to find blood vessels and a subdiffusive low-motility mode to find hotspots of invasion: pericytes.

**Intermittent search strategies—extensively reported at macroscopic and molecular levels—are now unveiled for a unicellular pathogen.**

# Threshold-free estimation of entropy from a Pearson matrix

Xi = $\{x_i^{(1)}, x_i^{(2)}, \ldots, x_i^{(n)}\}$, series i, taken into n time instants

EPL 141 (2023) 31003
Physicists + Neuroscientists

$$R_{ij} = \frac{1}{n}\sum_{k=1}^{n}\left[\frac{x_i^{(k)} - \langle x_i\rangle}{\sigma_i}\right]\left[\frac{x_j^{(k)} - \langle x_j\rangle}{\sigma_j}\right] = \frac{\langle X_i X_j\rangle}{\sigma_i\sigma_j}$$

Pearson correlation matrix

Usual: R → Adjacent matrix (of zeros and ones), then S is that of a network: $k_i$ degree of node i, then S = $\Sigma_i$ ln[$k_i$] / C, for C = N ln[N-1]

Ours: R → density matrix ρ, therefore we simply calculate S = -ρ ln[ρ]

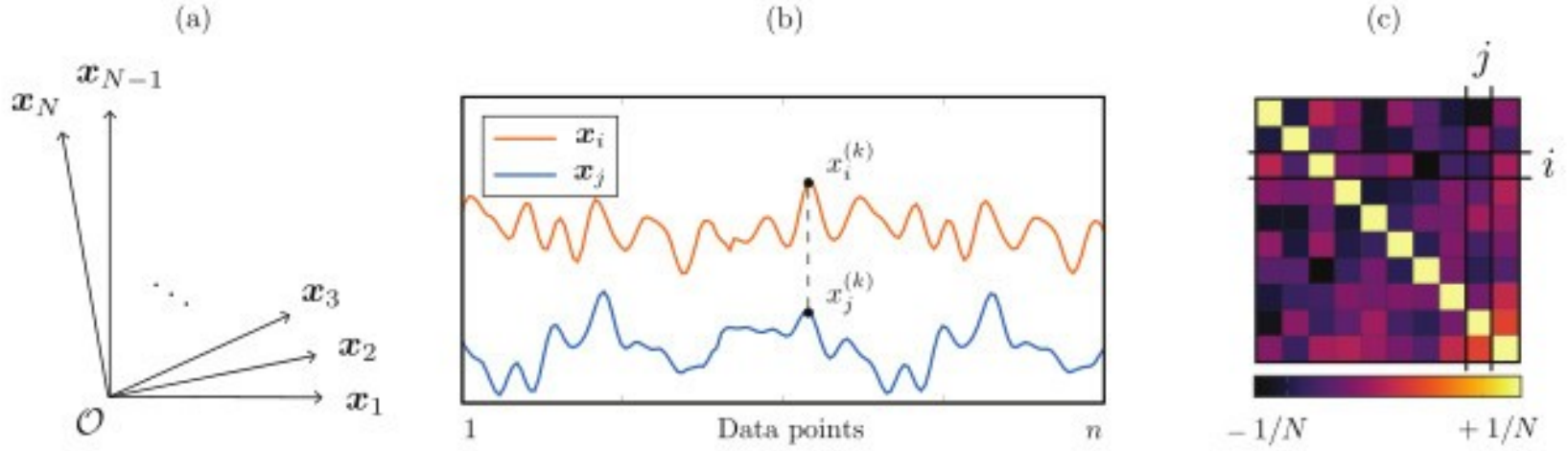


Fig. 1: The construction of a density matrix from a Pearson correlation matrix. (a) The system of interest is partitioned into $N$ interacting components or nodes. (b) The correlation between nodes $i$ and $j$ is then calculated. For each $i$ node there are $n$ data points $x_i^{(k)}$, where $k = 1, \ldots, n$. The correlation $R_{ij}$ between nodes $i$ and $j$ is given by eq. (3), and lies in the interval $-1 \leq R_{ij} \leq 1$. (c) For each correlation coefficient $R_{ij}$, we calculate $\rho_{ij} = R_{ij}/N$, yielding the matrix $\boldsymbol{\rho} = \boldsymbol{R}/N$. This matrix $\boldsymbol{\rho}$ fully satisfies the properties of a density operator, *i.e.*, i) hermiticity, ii) unit trace, and iii) positive semidefiniteness. Finally, we calculate the entropy from this density matrix via eq. (2).

# Threshold-free estimation of entropy from Pearson ... (cont I)

Entropic brain hypothesis: the entropy of spontaneous brain activity indexes the informational richness of conscious states. Hence, under certain chemical effects the entropy associated to neural activity may increase

Ayahuasca: indigenous beverage, a decoction with rapid antidepressant effects partially mediated by the serotonergic agonist N,N dimethyltryptamine (DMT)

A total of nine healthy human volunteers were assigned to a neuroimaging session both before and after ayahuasca intake. We obtained a set of N = 104 fMRI time series of the blood-oxygen-level–dependent (BOLD) signal of the human brain from each subject at both conditions.

# Threshold-free estimation of entropy from Pearson ... (cont II)

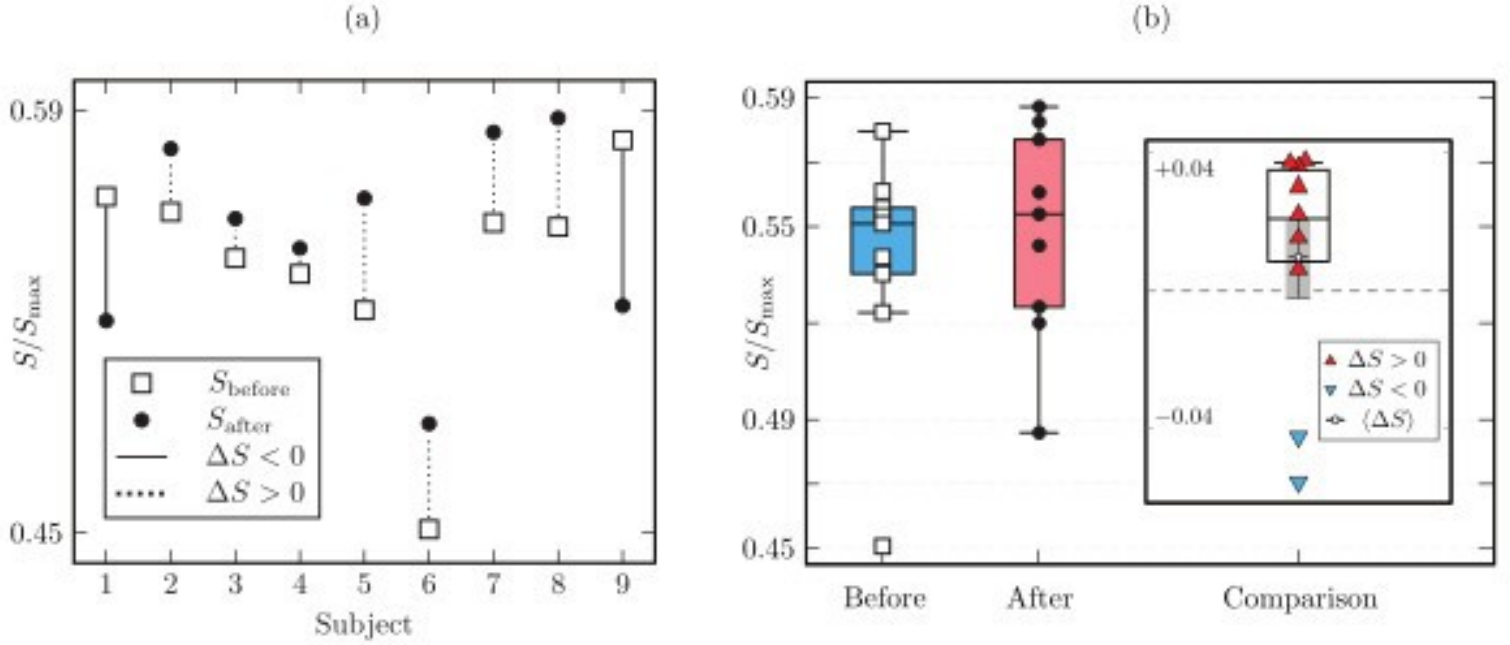


Fig. 4: Entropy before and after ayahuasca. (a) The plot shows the entropy $S$ of the nine subjects (horizontal axis), both before ($S_{\text{before}}$) and after ($S_{\text{after}}$) ayahuasca ingestion, normalized by $S_{\max} = \log(104)$. Entropy variation $\Delta S = S_{\text{after}} - S_{\text{before}}$ was found positive for seven subjects (dotted lines). (b) Box plots of the distribution $S_{\text{before}}$ and $S_{\text{after}}$, with the single outlier being subject 6 in the condition prior to ayahuasca consumption. On the right, the inset shows the box plot of the distribution of entropy variation. The error bar of the average $\langle \Delta S \rangle$ taken over all nine subjects is represented by the shaded region, and only slightly touches the $\Delta S < 0$ zone. These findings are broadly consistent with the hypothesis of psychedelic-induced brain entropy increase, although one must be careful due to the small number of subjects involved.

# Complex Systems Modeling

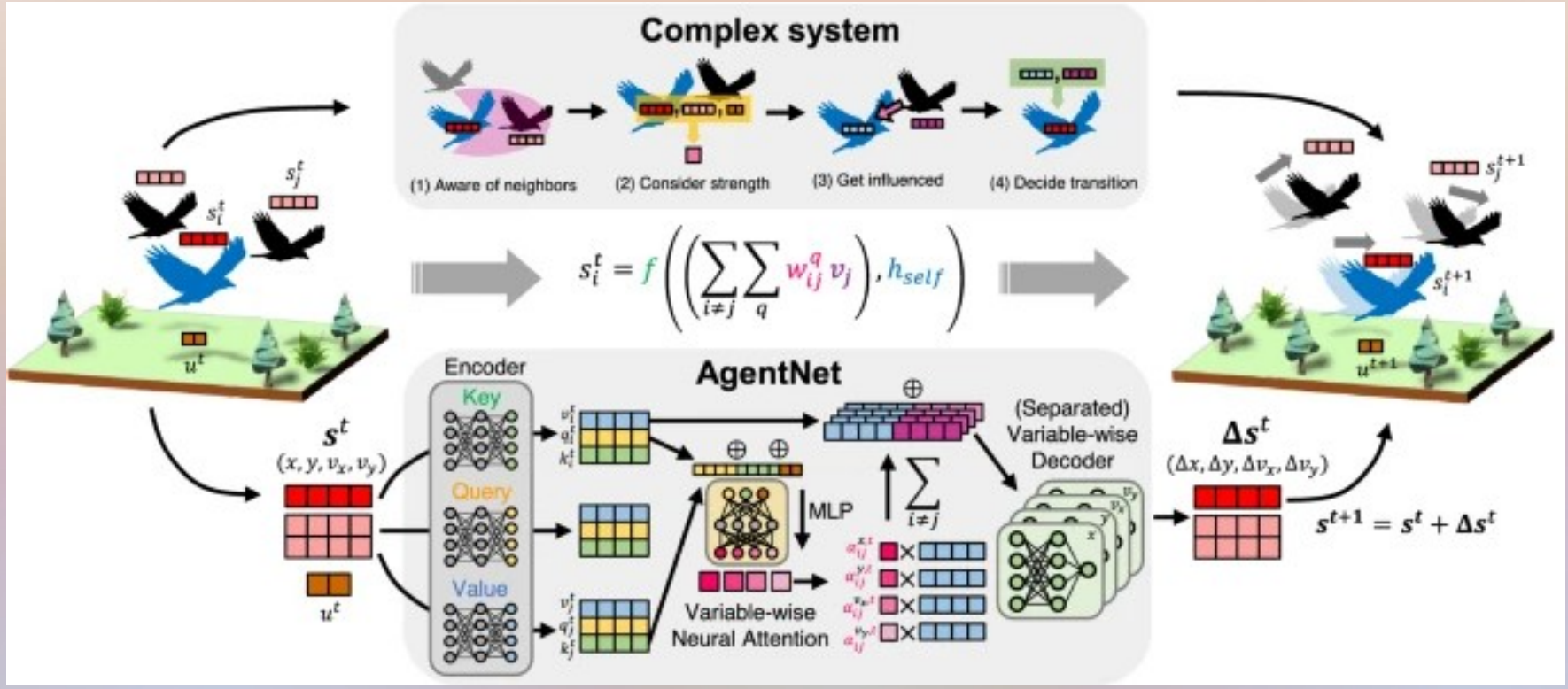


S. Ha and H. Jeong, Sc. Rep. 11 (2021) 12804

# Hey, but in Butkov and Arfken it is not like that!!!!

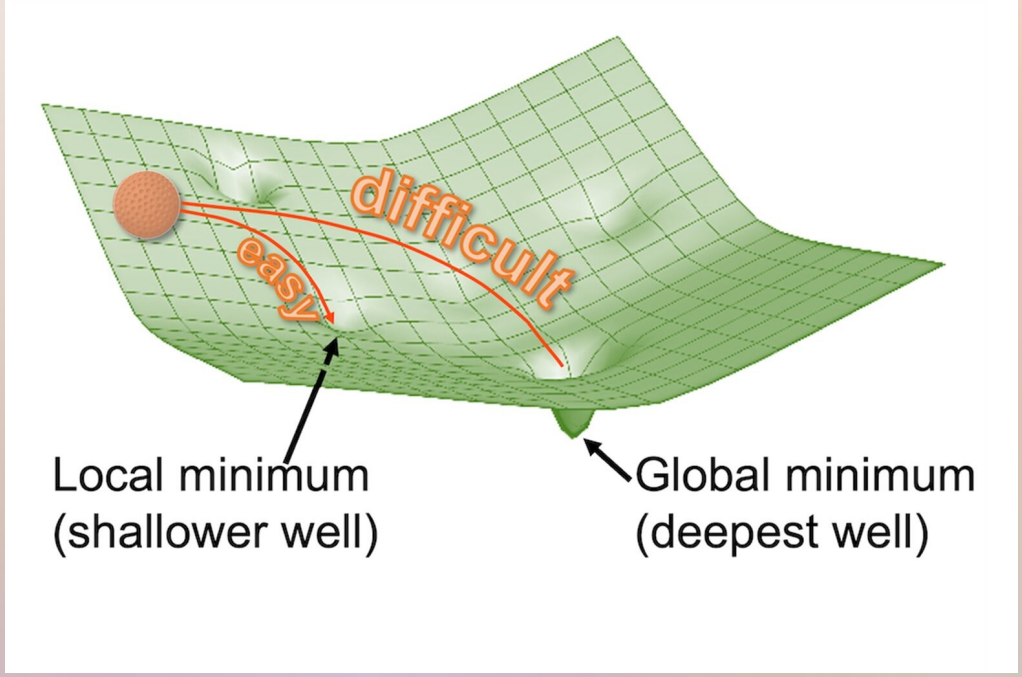


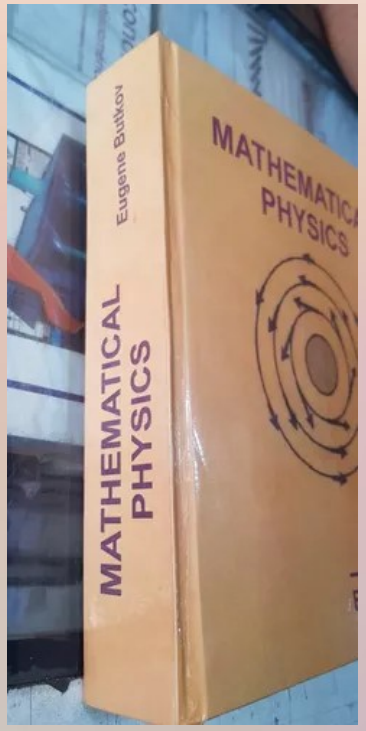


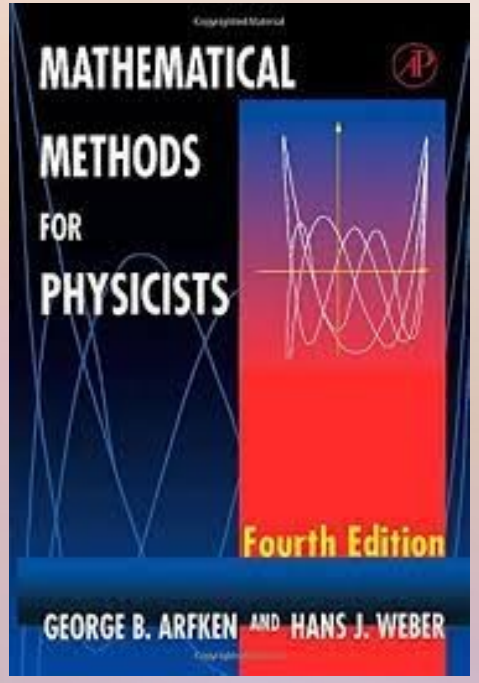


# What to do then???

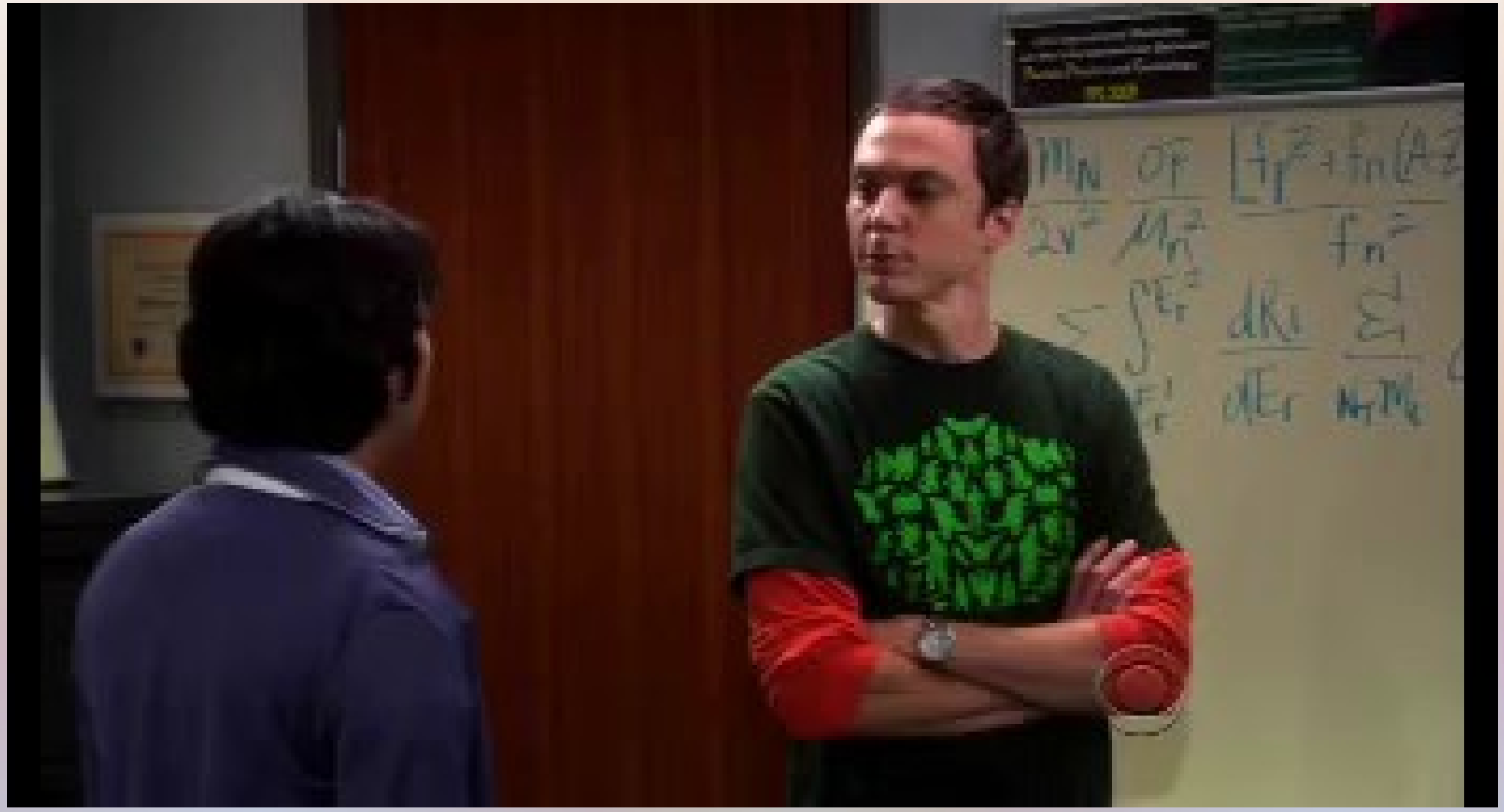

# Inside-outside duality for quantum billiards

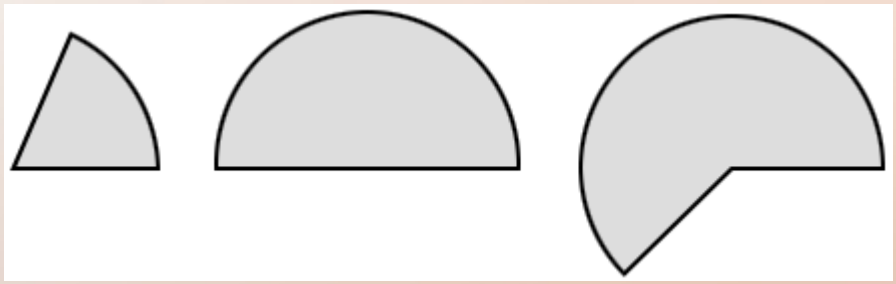

The billiard state is

$\sin[\pi\, l / \alpha] \quad J_{\pi\, l / \alpha}(k\, r)$.

But if $\pi\, l / \alpha$ is not rational, the wave function is not single valued in the whole plane.

The inside-outside duality (IOD): a billiard is invisible for a plane wave whose k equals the inside resonant k. But this fails for the above billiard, but why? IOD follows from the scattering S matrix, which is written as

$$S \sim \Sigma \int \text{functions} = \int \Sigma \text{functions}$$

But this fails if the functions are not uniformly convergent (for any x, ||f-fn|| are smaller than a certain ε for large enough n).

Applications: Wave Amplitude Gain
Azevedo, Maioli, Teston, Sales, Zanetti, Luz, PRE (2024) to appear.

# Lattice Green's funct., ST and Ising

M. A. G. Portillo, M. G. E. da Luz J. Phys. A 54 (2021) 325005; JSTAT (2022) 083208

- A graph is a very simple concept. For a given graph G(V,E) we define a spanning tree as a sub-graph without loops of G
- Suppose a regular periodic graph $G_n$, we can define the spanning tree constant as (for $|T_{Gn}|$ the number of spanning trees of $G_n$)

$$z_G = \lim_{n\to\infty} \ln[|T_{Gn}|] / |V(G_n)|$$

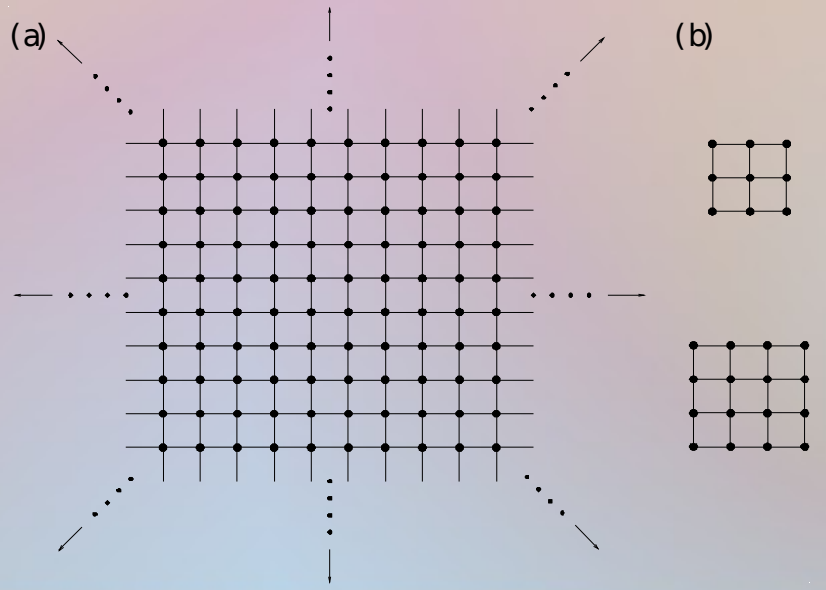


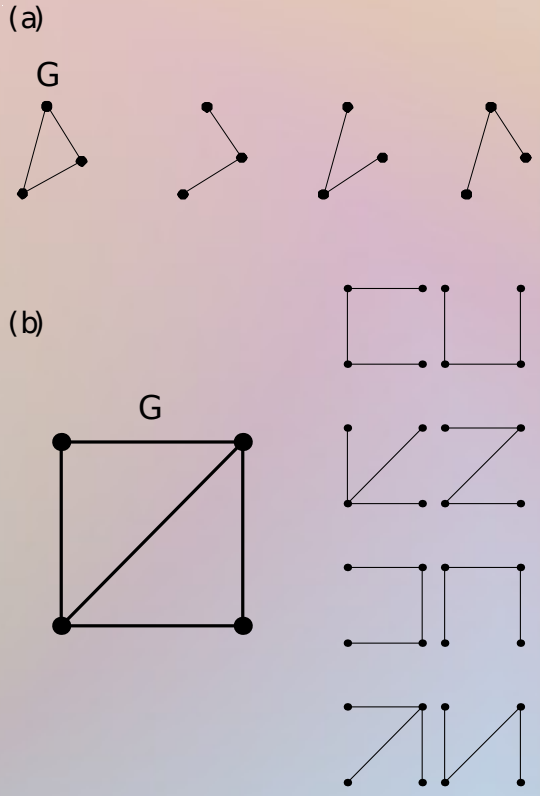

# Lat. Green's funct., ST and Ising – cont 1

Consider the Laplacian operator,

its lattice version is a simple discrete version of it:

$$\nabla^2 f(\mathbf{r}) \rightarrow D^2 f(\mathbf{r})$$

$$D^2 f(\mathbf{r}) = \sum_{\mathbf{a}} [f(\mathbf{r}+\mathbf{a}) + f(\mathbf{r}-\mathbf{a}) - 2 f(\mathbf{r})]/2$$

$$D^2 G(\mathbf{r}) = -\delta(\mathbf{r})$$

It is an amazing result in topology that the $z_G$ (spanning tree constant) can be calculated from the above G

Submitted PRE

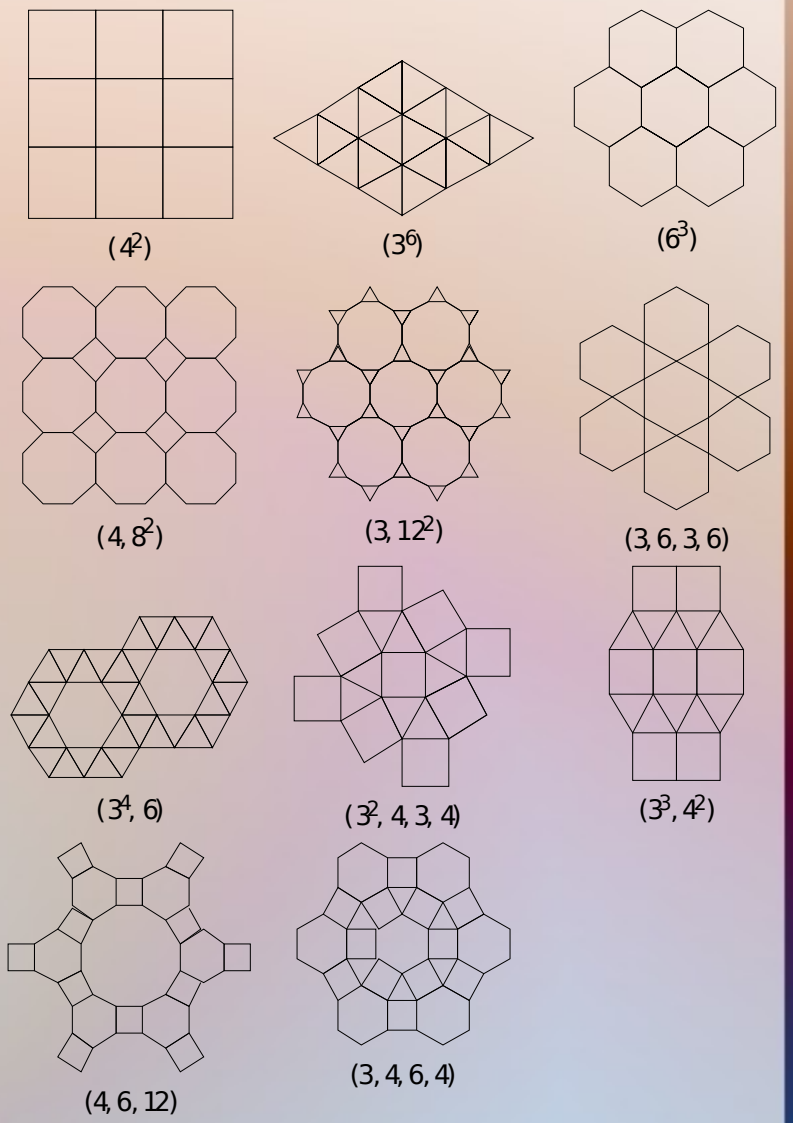


archimedean lattices

# Lat. Green's funct., ST and Ising – cont 2

Finally, from T(z) one calculates the partition function for many lattice models in physics

In particular for the Ising model

in different lattices, like below

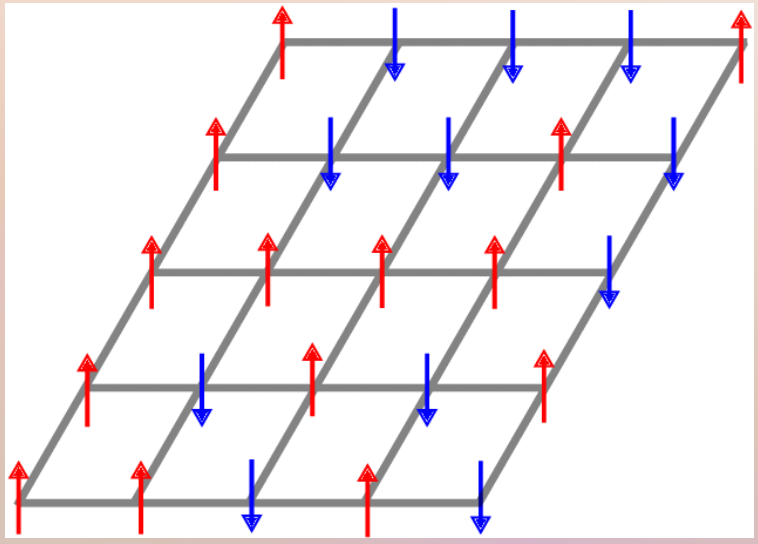

Martini

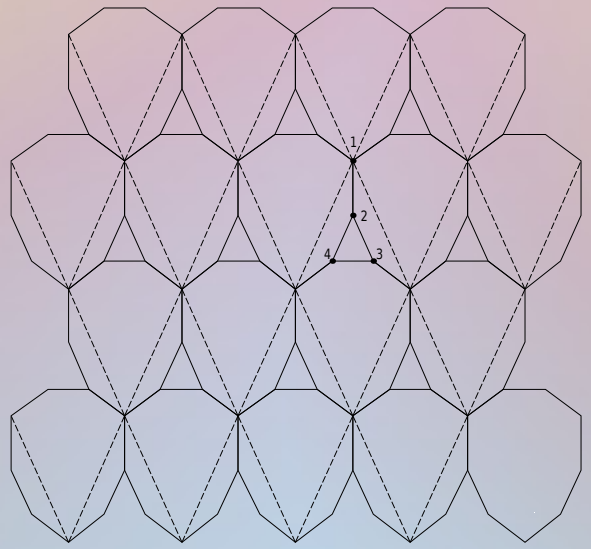


Covering/medial

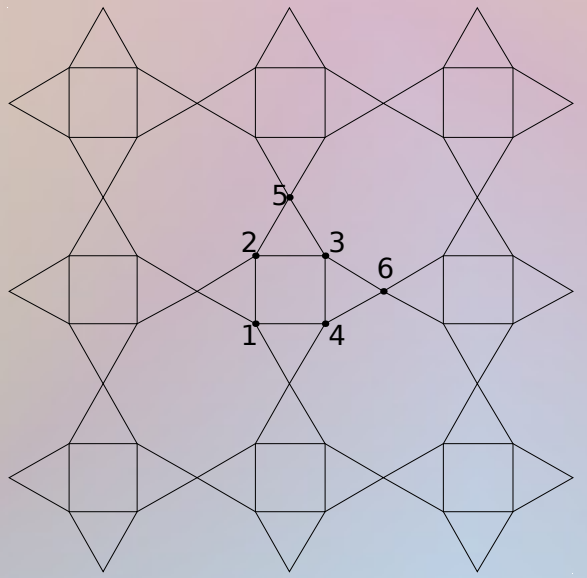

# Scattering quantum walk framework for two-dimensional materials: The case of honeycomb lattice structures

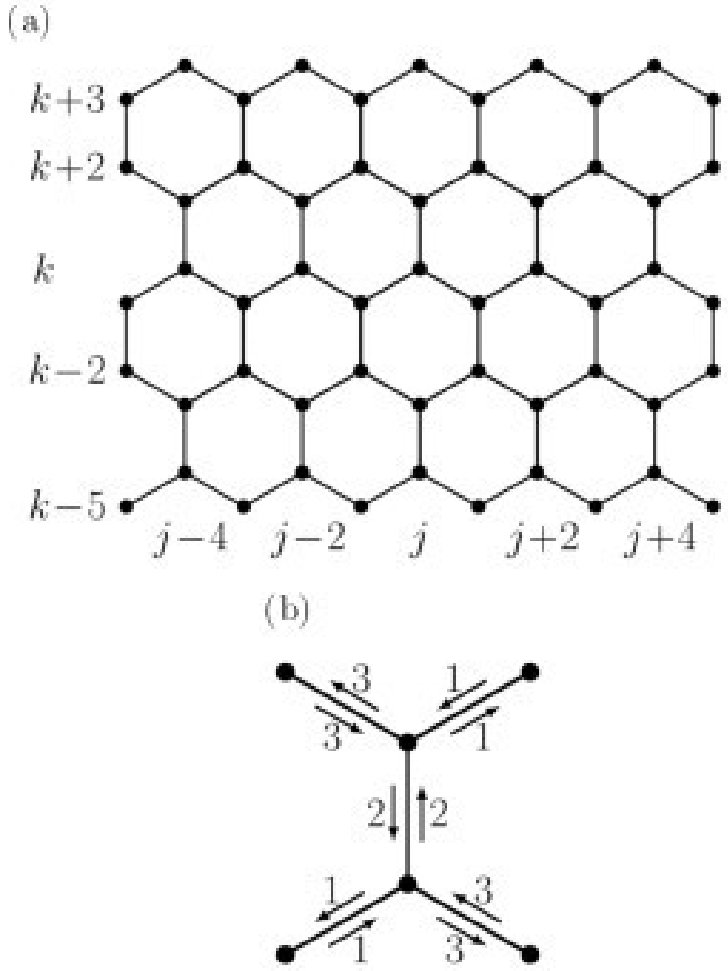


FIG. 1. (a) The honeycomb lattice. Without loss of generality, the $k$'s indicating the sites with one up and two down bonds are assumed even numbers. (b) The reference structure used to label (as indicated) the propagation direction quantum number $\sigma = 1, 2, 3$. Along each bond, two directions are possible.

$$x_j = \frac{\sqrt{3}\,j}{2}\,a, \qquad y_k = \left(\frac{3k}{4} + \frac{9-(-1)^k}{8}\right)a.$$

$$|\psi_n\rangle = \hat{U}^n |\psi_0\rangle$$

$$\hat{U}|\sigma, j, k\rangle = \sum_{\sigma'=1}^{3} \Gamma_{\sigma'\sigma}^{(j,k)} |\sigma', \mathcal{J}(\sigma', j, k), \mathcal{K}(\sigma', j, k)\rangle, \quad (4)$$

where $\mathcal{J}(\sigma', j, k)$ and $\mathcal{K}(\sigma', j, k)$ indicate the adjacent sites to $(j, k)$ through the direction $\sigma'$, or

$$\mathcal{J}(\sigma, j, k) = j + (\sigma - 2)(-1)^k,$$
$$\mathcal{K}(\sigma, j, k) = k + (-1)^{k+\sigma}. \quad (5)$$

$$\hat{\Gamma}^{(j,k)} = \hat{\Gamma}^{((-1)^k)}.$$

# Scattering quantum walk framework for two-dimensional materials: The case of honeycomb lattice structures (cont I)

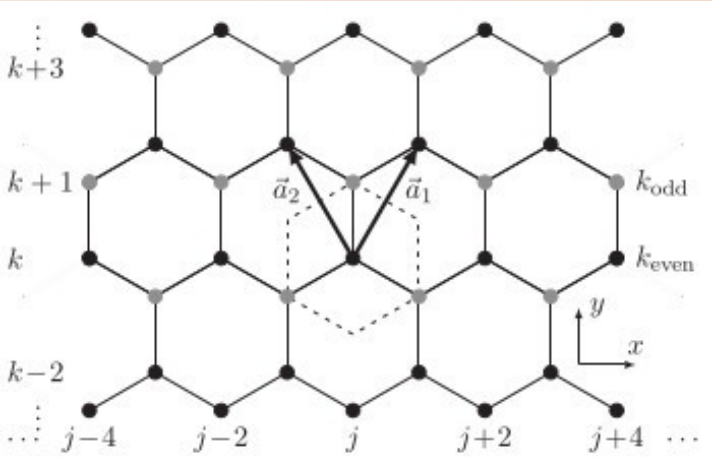


FIG. 8. The mapping of hexagonal lattice sites (black points) onto a triangular Bravais lattice (gray points). The area enclosed by the dashed line represents the Wigner-Seitz cell (WSc), whose translations by vectors $\vec{R}_{(m_1,m_2)}$—perpendicular to the WSc sides—cover the whole plane. The WSc contains two sites, both having the same $j$ coordinate. However, one of even and the other of odd $k$ coordinates.

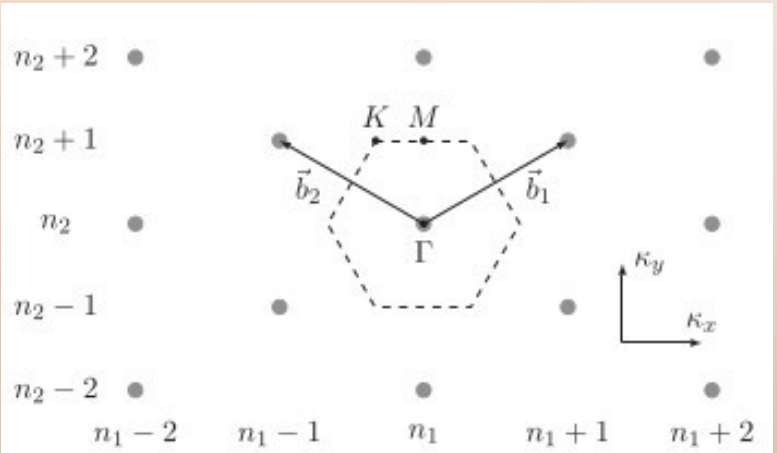


FIG. 9. The reciprocal associated with the Bravais lattice of Fig 8. Akin to the direct lattice, it is also triangular. The area enclosed by the dashed hexagon delimits the first Brillouin zone. The points of high symmetry, Γ, $K$, and $M$, have, respectively, the coordinates, (0,0), $(-\frac{2\pi}{3\sqrt{3}a}, \frac{2\pi}{3a})$ and $(0, \frac{2\pi}{3a})$.

$$\det(\hat{F}\,\hat{\Gamma}^{(-)}\hat{F}^{\dagger}\,\hat{\Gamma}^{(+)} - \exp[-2iE/\hbar]\,\hat{\mathbf{1}}) = 0,$$

$$F_{\sigma\sigma} = \exp\left[i\,a\left(\frac{\sqrt{3}}{2}\kappa_x\,\sigma + \frac{3}{4}\kappa_y\,(-1)^{\sigma}\right)\right]$$

# Scattering quantum walk framework for two-dimensional materials: The case of honeycomb lattice structures (cont II)

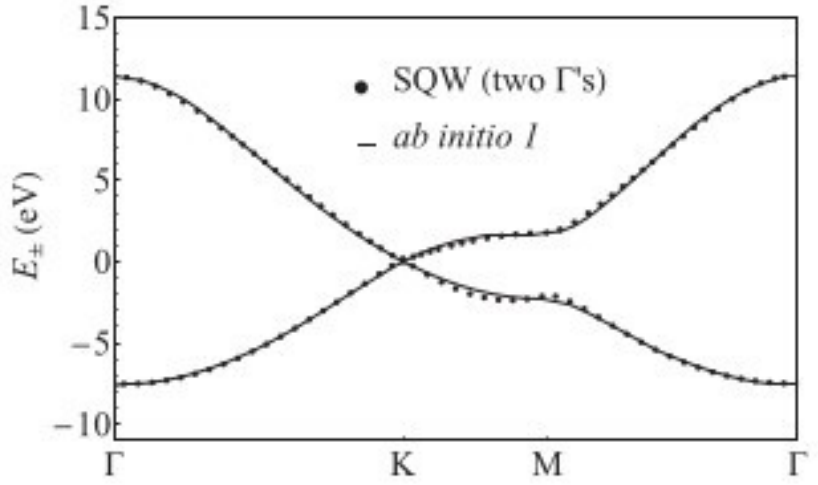


FIG. 18. The graphene energy band structures from Eq. (29), with $\Gamma^{(+)} \neq \Gamma^{(-)}$ (see main text). The results are compared with those from the *ab initio* 1 method [36].

PRB 108 (2023) 094303
B. F. Venancio, H. S. Ghizoni, M. G. E. da Luz

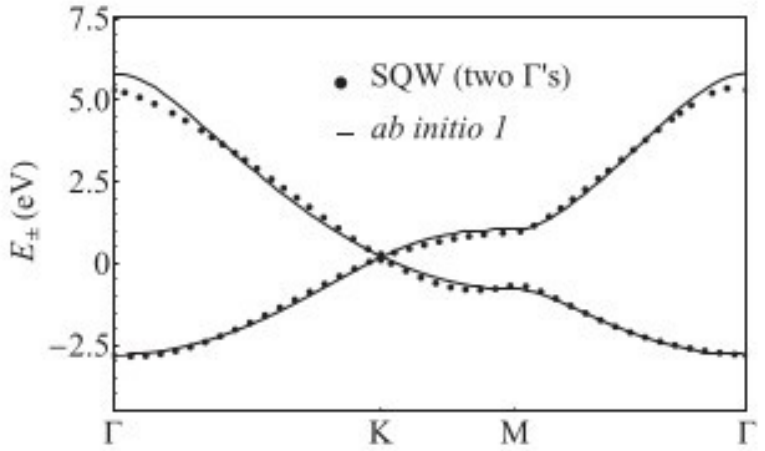


FIG. 19. The same than in Fig. 18, but for the planar germanene.

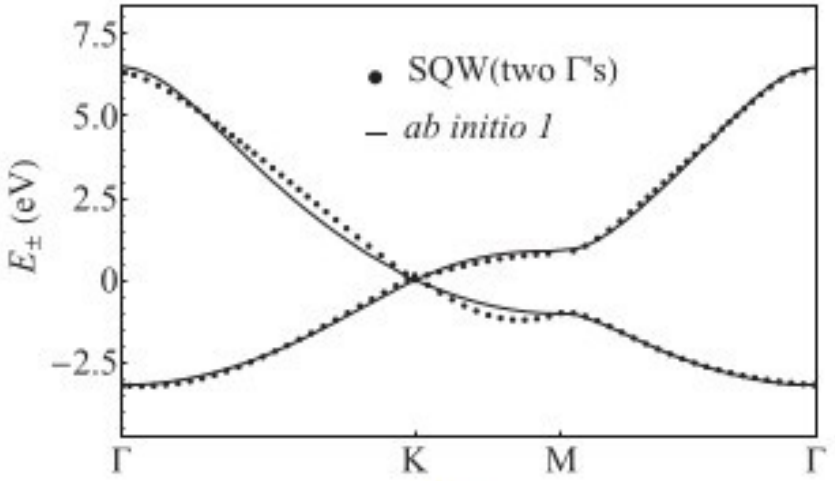


FIG. 20. The same than in Fig. 18, but for the planar silicene.

# Lattice Thermal Conductivity of 2D Nanomaterials: A Simple Semi-Empirical Approach

R. M. Tromer, I. M. Felix, L. F. C. Pereira, M. G. E. da Luz, L. A. Ribeiro Jr., D. S. Galvão, PCCP 25, 28703 (2023)

Fourier law in 3D: $J_i = \sum_j \kappa_{ij} (\nabla T)_j$ where

$J_i$ the heat current in the i direction, $(\nabla T)_j$ the temperature gradient in the j direction and $\kappa_{ij}$ the i j element of the heat conductivity tensor

We write $J = (J_x + J_y)/2$, for (assuming a same temperature variation in all directions)

$$J_x \approx \kappa_{xx} \delta T / \delta x + \kappa_{xy} \delta T / \delta y + \kappa_{xz} \delta T / \delta z$$

$$J_y \approx \kappa_{yx} \delta T / \delta x + \kappa_{yy} \delta T / \delta y + \kappa_{yz} \delta T / \delta z$$

Now, we phenomenologically relate the heat current J to the delivered power W across the effective area L δz, representing a kind of average of the areas δx δz (normal to $J_y$) and δy δz (normal to $J_x$), so that $J = W/(L \delta z)$. Importantly, L is a “characteristic length”.

# Lattice Thermal Conductivity of 2D Nanomaterials: A Simple Semi-Empirical Approach (cont I)

$$\frac{W}{L\,\delta_z} \approx \left[\frac{(\kappa_{xx}+\kappa_{yx})}{2}\frac{1}{\delta_x} + \frac{(\kappa_{xy}+\kappa_{yy})}{2}\frac{1}{\delta_y} + \frac{(\kappa_{xz}+\kappa_{yz})}{2}\frac{1}{\delta_z}\right]\delta T,$$

$$\frac{W}{L\,\delta T} \approx \boxed{\left[\frac{(\kappa_{xx}+\kappa_{yx})}{2}\frac{\delta_z}{\delta_x} + \frac{(\kappa_{xy}+\kappa_{yy})}{2}\frac{\delta_z}{\delta_y}\right]} + \frac{(\kappa_{xz}+\kappa_{yz})}{2}\Bigg].$$

$\kappa_L$

Extra key assumptions: $\kappa_{ij}$ (i, j not z) scales inversely with $\delta z$. Hence, for $\delta z \rightarrow 0$ we suppose the product $\kappa_{ij}\,\delta z$ to be well behaved and finite. Also, in such limit, we also expect $\kappa_{iz}$ and $\kappa_{zj}$ to vanish. So that we have a $\kappa_L$ and

$$\kappa_L = W / (L\,\delta T) \quad \rightarrow \quad \kappa_L = \nu\ E / (L\,\delta T)$$

# Lattice Thermal Conductivity of 2D Nanomaterials: A Simple Semi-Empirical Approach (cont II)

- ν → vibrational models of the "artificial molecule"
- E → average energy, an Arrhrenius-like fitting
- δT → machine learning or fitting models

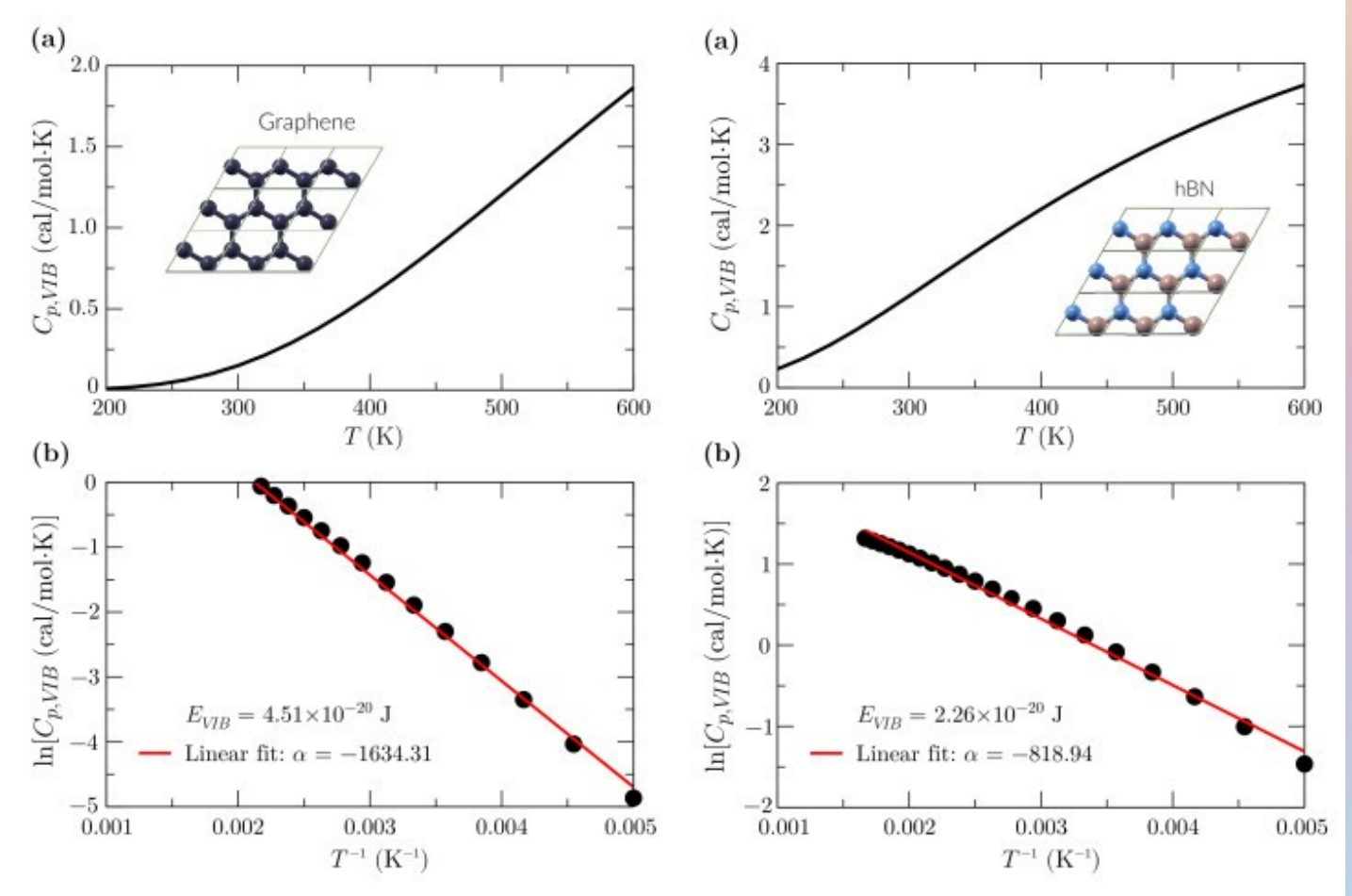

# Lattice Thermal Conductivity of 2D Nanomaterials: A Simple Semi-Empirical Approach (cont III)

TABLE I. Thermochemical results, method parameters, and lattice parameters for all the studied 2D nanomaterials. Here, $\kappa_{ref.}$ relates to pertinent values obtained in the literature.

| Structure | Method | $N_{atom}$ | $\bar{\omega}$ ($cm^{-1}$) | $\alpha$ | $E_{VIB}$ ($10^{-21}$ J) | $L$ (Å) | $\delta T$ (K) | $\kappa$ (W/m·K) | $\kappa_{ref.}$ (W/m·K) |
|---|---|---|---|---|---|---|---|---|---|
| Graphene | PM7 | 2 | 1709.85 | -1634.3 | 45.1 | 2.5 | 3 | 3084.6 | 3000 – 5000[40,81,82] |
| Graphene | AM1 | 2 | 1761.65 | -1699.5 | 46.9 | 2.5 | 3 | 3304.8 | 3000 – 5000[40,81,82] |
| hBN | PM7 | 2 | 963.3 | -818.9 | 19.3 | 2.5 | 9 | 289.2 | 220 – 550[83–86] |
| Phagraphene | PM7 | 20 | 1123.89 | -457.8 | 12.6 | 7.2 | 3 | 196.7 | 218x/285y/251.5[87] |
| Phagraphene | AM1 | 20 | 1188.37 | -465.4 | 12.8 | 7.2 | 3 | 211.3 | 218x/285y/251.5[87] |
| $WS_2$ | PM7 | 3 | 475.62 | -390.736 | 10.8 | 3.2 | 15 | 32.1 | 32.0[88] |
| $MoS_2$ | PM7 | 3 | 325.41 | -313.3 | 8.65 | 3.2 | 15 | 17.6 | 34.5[41] |
| $MoS_2$ | AM1 | 3 | 367.89 | -307.8 | 8.50 | 3.2 | 15 | 19.5 | 34.5[41] |
| Silicene | AM1 | 2 | 419.54 | -170.4 | 4.70 | 3.9 | 15 | 10.1 | 9.4[89–91] |
| Germanene | MNDO | 2 | 424.15 | -170.8 | 4.71 | 4.0 | 15 | 10.0 | 2.4[91,92] |
| Ene-yne | PM7 | 20 | 993.17 | -282.0 | 7.78 | 10.4 | 15 | 14.9 | 10x/3y/6.5[93–95] |
| Ene-yne | AM1 | 20 | 993.71 | -293.9 | 8.11 | 10.4 | 15 | 15.5 | 10x/3y/6.5[93–95] |
| Pentagraphene | PM7 | 6 | 1099.75 | -703.116 | 19.4 | 3.64 | 15 | 117.2 | 167.0[96] |
| Pentagraphene | PM3 | 6 | 1171.57 | -730.96 | 20.2 | 3.64 | 15 | 130.0 | 167.0[96] |
| Graphenylene/D-graphene | PM7 | 12 | 1069.83 | -468.7 | 12.9 | 6.7 | 3 | 206.0 | 600.0[97] |
| T-graphene | PM7 | 4 | 1999.03 | -244.66 | 6.75 | 3.11 | 3 | 433.9 | 800.0[97] |
| Biphenylene-network | PM7 | 6 | 1033.76 | -457.36 | 12.6 | 4.09 | 3 | 318.5 | 208.3/240.0[98] |
| Biphenylene-network | PM3 | 6 | 1114.09 | -346.16 | 9.55 | 4.09 | 3 | 260.1 | 208.3/240.0[98] |
| NHG | PM7 | 18 | 1010.94 | -389.8 | 10.7 | 8.3 | 6 | 65.2 | 64.5[99,100] |
| Borophene-$\beta$ | PM7 | 5 | 621.08 | -256.6 | 7.08 | 4.1 | 3 | 107.2 | 90.0[101] |
| Phosphorene | PM7 | 4 | 609.55 | -191.63 | 5.29 | 3.96 | 15 | 16.3 | 30.15x/13.65y/21.9[10 |
| $BC_3$ | PM7 | 8 | 996.72 | -440.4 | 12.2 | 5.2 | 6/4 | 467.7 | 410[76] |
| $BC_6N-1$ | PM7 | 8 | 1037.00 | -424.3 | 11.7 | 5.0 | 3/5 | 1213.3 | 1080.0[76] |
| $BC_6N-2$ | PM7 | 8 | 1050.64 | -458.0 | 12.6 | 5.0 | 3/6 | 1588.6 | 1570.0[76] |
| BAS | PM7 | 2 | 648.87 | -376.4 | 10.0 | 3.4 | 3 | 190.8 | 180.2[103] |
| Diboron-porphyrin | PM7 | 26 | 1042.19 | -454.68 | 12.5 | 8.4 | 3 | 155.1 | 160x/115y/137.5[78] |
| $PtS_2$ | PM6 | 3 | 466.46 | -372.47 | 10.3 | 3.6 | 3 | 133.5 | 85.6[104] |
| KCuTe | PM7 | 6 | 159.78 | -63.10 | 1.74 | 4.44 | 15 | 1.3 | 0.13[105] |
| GaTe | PM7 | 4 | 196.83 | -155.8 | 4.30 | 4.1 | 15 | 4.1 | 5.2[106] |
| 2D-$qHC_{60}$ | PM7 | 60 | 1031.03 | -496.8 | 13.7 | 9.2 | 75 | 6.1 | 4.3[107] |
| 2D-$C_{36}$ | PM7 | 36 | 1045.11 | -510.7 | 14.1 | 7.6 | 75 | 7.7 | 9.8[108] |

# Muito obrigado Curitiba



**By the way, in case of any question, ask Mr. Light**